

## The Community Climate System Model, Version 2

JEFFREY T. KIEHL AND PETER R. GENT

*National Center for Atmospheric Research,\* Boulder, Colorado*

(Manuscript received 11 November 2003, in final form 6 April 2004)

### ABSTRACT

The Community Climate System Model, version 2 (CCSM2) is briefly described. A 1000-yr control simulation of the present day climate has been completed without flux adjustments. Minor modifications were made at year 350, which included all five components using the same physical constants. There are very small trends in the upper-ocean, sea ice, atmosphere, and land fields after year 150 of the control simulation. The deep ocean has small but significant trends; however, these are not large enough that the control simulation could not be continued much further. The equilibrium climate sensitivity of CCSM2 is 2.2 K, which is slightly larger than the Climate System Model, version 1 (CSM1) value of 2.0 K.

Several aspects of the control simulation's mean climate and interannual variability are described, and good and bad properties of the control simulation are documented. In particular, several aspects of the simulation, especially in the Arctic region, are much improved over those obtained in CSM1. Other aspects, such as the tropical Pacific region simulation, have not been improved much compared to those in CSM1. Priorities for further model development are discussed in the conclusions section.

### 1. Introduction

The first version of the Climate System Model (CSM1) was developed mainly at the National Center for Atmospheric Research (NCAR) and was released in 1996. A 300-yr fully coupled control simulation was performed that had a stable upper-ocean, sea ice, atmosphere, and land climatology. This was the first such simulation obtained without the use of flux adjustments (see Boville and Gent 1998). There was a second release in 1998 that improved the software and corrected the air-sea ice drag coefficient, which was much too large in the original code. CSM, version 1.3 (CSM1.3), released in 2000, contained physics improvements in all components for use in transient climate simulations (see Boville et al. 2001).

Since then, work has continued to develop a second version of the model with the involvement of many scientists from both the academic community and other national laboratories. In recognition of this fact, the new model has been renamed the Community Climate System Model, version 2 (CCSM2). Completely new land and sea ice components have been developed that are

briefly described below, and the ocean component has a new base code. One reason for these changes and choices is that CCSM2 now runs efficiently on massively parallel computers, while the first version did not. A considerable amount of software engineering work has been done on the CCSM2 components and the coupler to make the code portable and efficient on a variety of platforms and easier to understand and run. Much of this work has been done in collaboration with several scientists at institutions funded by the Department of Energy. The CCSM2 project is jointly funded by the National Science Foundation and the Department of Energy.

The CCSM2 components are briefly described in section 2. Sections 3 and 4 describe the control simulation mean climatology and interannual variability. A discussion and conclusions are given in section 5.

### 2. Model formulation

#### *a. The CCSM2 atmosphere component*

The atmosphere component of CCSM2 is the Community Atmosphere Model version 2.0 (CAM2.0). This model is the successor of version 3 of the Community Climate Model (CCM3; Kiehl et al. 1998). The model employs a spectral dynamical core as in CCM3 with a T42 horizontal resolution. CAM2.0 has 26 vertical levels as compared to the 18 levels defined in CCM3. The additional eight levels were added near the tropopause to better define large-scale cross-tropopause transport.

---

\* The National Center for Atmospheric Research is sponsored by the National Science Foundation.

---

*Corresponding author address:* Dr. Jeffrey T. Kiehl, National Center for Atmospheric Research, 1850 Table Mesa Drive, Boulder, CO 80305.  
E-mail: jtkon@ucar.edu

CAM2.0 includes a number of improvements to the physical parameterizations. The diagnostic cloud water scheme of CCM3 has been replaced with a prognostic scheme for total cloud condensate and is described in Rasch and Kristjansson (1998). Total water is predicted for a model grid box, and based on the grid box temperature, this condensate is partitioned between liquid and ice. Cloud fraction is still diagnosed similarly to CCM3. Given the increased vertical level structure, a new cloud overlap methodology was developed by Collins (2001). This approach provides a generalized scheme to treat the overlap of cloud layers. The CAM2.0 configuration assumes that clouds are maximally overlapped when in adjacent layers and randomly overlapped when there is a gap in between cloud layers.

CAM2.0 also employs the updated cloud water vapor emissivity/absorptivity scheme by Collins et al. (2002). This new treatment of the longwave properties of water vapor includes version 2.1 of the Clough–Kneizys–Davies (CKD) continuum developed by Clough et al. (1989). This improvement brings the modeled longwave fluxes and cooling rates into better agreement with detailed line-by-line calculations. It has a significant impact in enhancing longwave cooling in the upper troposphere, which in turn affects the behavior of the convective parameterization. Briefly, the change in convective activity led to a significant drying of the atmosphere, especially in the Tropics. To alleviate this degradation in the modeled hydrologic cycle, a change was made to include the evaporation of convective precipitation back to the atmosphere, that is, not all convective precipitation reaches the surface. A profile of the precipitate is produced by the moist convection process; the evaporation of this precipitate back into the atmosphere is directly proportional to the large-scale relative humidity in a given model layer. The change in the longwave scheme also addressed a longstanding bias in the polar regions where the original CCM3 clear-sky downward flux was too low. The CAM2.0 polar clear-sky longwave surface fluxes are now in very good agreement with observations.

Further enhancements to the uncoupled CAM2.0 include the inclusion of a new ozone dataset documented in Kiehl et al. (1999); the use of the thermodynamic component of the CCSM sea ice model, version 4 (CSIM4); the use of the new Community Land Model, version 2.0 (CLM2.0); and the implementation of realistic fractional land, ocean, and sea ice for grid boxes. The model also includes the capability of employing a reduced grid at high latitudes for computational efficiency.

Improvements in the climate simulation of the uncoupled CAM2.0 model compared to the climatology simulated by CCM3 include a more realistic distribution and amount of precipitable water, an improved clear longwave flux simulation compared to observations, an improved shortwave cloud forcing in the regions of cold sea surface temperatures (SSTs) at eastern ocean bound-

aries, and a reduction in central American convective activity with an associated improvement in surface wind stress in the subtropics. There are a number of areas where the CAM2.0 simulation has degraded the simulation compared to that of CCM3. These include a colder tropical tropopause, a significant warm bias over land at high latitudes, and a tendency to produce a double intertropical convergence zone (ITCZ) structure in the uncoupled mode, that is, with prescribed sea surface temperatures. These are significant biases in the model, and they increase in magnitude when CAM2.0 is coupled to the ocean, land, and sea ice components.

#### *b. The CCSM2 ocean component*

The ocean component uses the Parallel Ocean Program (POP) code, which was developed at the Los Alamos National Laboratory (see Smith et al. 1992). The ocean grid uses spherical coordinates in the Southern Hemisphere, but in the Northern Hemisphere, the pole is displaced into Greenland at 80°N, 40°W. The horizontal grid has 320 × 384 grid points, and the resolution is uniform in the zonal, but not in the meridional, direction. In the Southern Hemisphere, the meridional resolution is 0.27° at the equator, gradually increasing to 0.54° at 33°S, and is constant at higher latitudes. There are 40 levels in the vertical; the first 5 in the upper ocean are 10 m thick, and below 50 m the resolution coarsens, with the bottom level being 250 m thick. The minimum depth is 30 m, and the maximum depth is 5.5 km. The horizontal viscosity is a Laplacian operator that is anisotropic and uses different coefficients in the zonal and meridional directions (see Smith and McWilliams 2003). Both coefficients are spatially variable and depend on the local rates of shear and strain based on the scheme of Smagorinsky (1963). The time step used is just less than 1 h, which is small enough that no Fourier filtering is required around the Greenland pole. This is a significant improvement over CSM1, because its ocean component used spherical coordinates in the Northern Hemisphere, which required strong numerical filtering in the Arctic Ocean around the North Pole.

The vertical mixing scheme is the *K*-profile parameterization scheme of Large et al. (1994) that was used in the ocean component of the CSM1. The parameterization of the effects of mesoscale eddies is that of Gent and McWilliams (1990). It mixes along isopycnals with a Laplacian operator and uses an additional advection of temperature and salinity. This parameterization is implemented as a skew-diffusion term using the very accurate numerical algorithm that is described in Griffies (1998). The ocean component also uses a new, and very accurate, equation of state for seawater that is documented in McDougall et al. (2003). The sea surface height varies locally, but the ocean volume remains fixed. Therefore, the surface freshwater flux is converted into an implied salt flux using a constant reference salinity of 34.7 practical salinity units (psu). The ocean

component is fully documented in the scientific reference manual (see Smith and Gent 2002).

### c. The CCSM2 land component

The land component of CCSM2 is the CLM2.0. This model was created by a large group of community developers and is described in detail in Bonan et al. (2002). Briefly, CLM2 includes improved biogeophysical parameterizations compared to the earlier Land Surface Model (LSM) of Bonan (1998). CLM2 combines a number of the features of LSM and the biosphere–atmosphere transfer scheme (BATS) model of Dickinson et al. (1993). CLM2 includes a 10-layer model for soil temperature and soil water and distinguishes between liquid and ice phase in the soil water. It also includes a multilayer model of snowpack and a state-of-the-art river runoff model. The river runoff scheme is based on the work of Branstetter and Erickson (2003). The scheme calculates and routes runoff realistically on a  $0.5^\circ$  grid. At the model coasts, the runoff can either be distributed directly into a small area of the active ocean domain or into a marginal sea. The area-averaged water flux into these marginal seas is balanced, and the excess or deficit of water is included in a small area of the adjacent active ocean as an implied surface salt flux. Marginal seas are the Baltic, Black, Caspian, and Red Seas. The model also includes new formulations of ground and vegetation fluxes and the vertical root profile of Zeng (2001). Five basic subgrid land types (glacier, lake, wetland, urban, and vegetated) represent a CLM2 grid box. The vegetation is further refined into 4–16 plant functional types.

The changes in CLM2 have addressed significant biases that existed in the previous versions of the land surface model. In particular, the new land model results in warmer surface air temperatures in all seasons. There are also significant improvements in the simulated land hydrologic cycle (see Bonan et al. 2002 for details).

### d. The CCSM2 sea ice component

The new sea ice component (CSIM4) uses the elastic–viscous–plastic ice rheology of Hunke and Dukowicz (1997). The thermodynamics module consists of an explicit brine-pocket parameterization based on Bitz and Lipscomb (1999) and an ice thickness distribution module described in Bitz et al. (2001). There are five ice thickness categories, with the thinnest having a maximum thickness of 64 cm. The remapping between thickness categories uses the scheme of Lipscomb (2001). The sea ice component uses the same displaced Greenland pole grid as the ocean component, and again no numerical filtering of the solution is needed. Details of CSIM4 and simulations using it are described in Briegleb et al. (2004).

There have been changes in the coupler compared to CSM1, although it still acts as the driver controlling the

four components of CCSM2. However, the fluxes between the atmosphere and the new land and sea ice components are now calculated in the new components and passed to the atmosphere every hour. Thus, these fluxes resolve the diurnal cycle. In contrast, the atmosphere–ocean fluxes are calculated in the coupler, and communication between these components occurs once every day. Most of the control simulation was run on 144 processors of the IBM SP supercomputer at the National Energy Research Scientific Computing Center (NERSC). The simulation executed at almost five years per calendar day and took 7 months to complete 1000 yr.

## 3. The control simulation

The ocean component of the control simulation was initialized using temperature and salinity fields from observations. Over most of the ocean, the January mean fields from Levitus et al. (1994) were used. However, the Arctic Ocean was initialized using the poles data (see Steele et al. 2001) because it is more realistic and has fewer problems with unstable density profiles. The atmosphere, land, and sea ice components were initialized using realistic January fields obtained from stand-alone integrations of these three components. This is a completely different initialization strategy than that used for CSM1. The advantage of the present choice is that the ocean starts from a more realistic initial condition. The disadvantage is that trends in the ocean simulation must occur over long time scales as it adjusts from the initial condition toward its equilibrium solution.

Atmospheric gas concentrations for the control simulation are set at 1990 levels. The atmospheric  $\text{CO}_2$  volume mixing ratio is set to 355 ppmv. This control simulation was run for 350 yr without any flux adjustments. Then three changes were made to the code, which will be discussed below, and the simulation was restarted and run out to year 1000, again with no flux adjustments. The first of the changes was to ensure that all five modules of CCSM2 were using the same set of shared constants. In many cases, this simply ensured that “constants” such as  $\pi$  were the same in all components. However, for other constants, different choices had been made in the various components, mostly because these constants are really slowly varying functions of temperature, pressure, etc. The largest change to the coupled simulation due to sharing constants arose because the latent heat of vaporization used in the atmosphere component changed by about 1%. The atmosphere determines the latent heat flux by multiplying the water vapor flux sent to it from the coupler by the latent heat of vaporization  $L$ . Thus, changing  $L$  implied a different latent heat flux for a given water vapor flux.

Figure 1 shows the time series of the global annually averaged surface temperature for the entire 1000-yr simulation. There is an initial spin up in temperature of around 150 yr that is associated with adjustments in sea

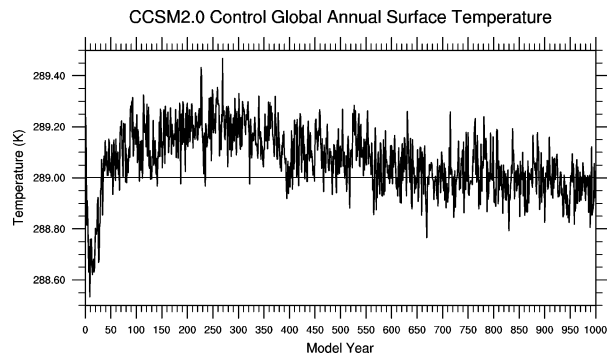


FIG. 1. Time series of the global annually averaged surface temperature (K) from the 1000-yr CCSM2 control integration. The solid horizontal line is the average surface temperature for the last 400 yr of the integration.

ice. There is a decrease in surface temperature at year 350 associated with the change in shared constants. The surface comes into a stable equilibrium after another 200–300 yr. Figure 2 shows the heat balance at the top of the atmosphere and at the surface, and the difference between them over the 1000-yr simulation. The net imbalance averages  $0.5 \text{ W m}^{-2}$  over the first 350 yr but

then reduces to  $0.2 \text{ W m}^{-2}$ , mostly due to the changed  $L$  in the atmosphere described above. The subsequent imbalance of  $0.2 \text{ W m}^{-2}$  is similar to the imbalance in atmosphere-alone runs. Most of this imbalance occurs because the latent heat of fusion is not released when snow is formed from water. In the land and sea ice components, heat is required to melt the snow received from the atmosphere, so that the coupled system has a net sink of heat. For most of the 1000-yr run, the atmosphere is close to balanced at the surface, so that the heat for this sink comes from the ocean. Figure 3 shows the volume-averaged potential temperature from the ocean over the 1000-yr run. Over the first 100 yr, the ocean temperature increases from its initial condition of  $3.64^\circ\text{C}$ . Then there is a monotonic heat loss for the remainder of the simulation, with the final temperature being  $3.11^\circ\text{C}$  at year 1000. A break in the slope can be seen at year 350, but the slope gradually decreases and the average rate of ocean heat loss over the last 300 yr is about  $0.25 \text{ W m}^{-2}$ . We note that, even though the ocean heat content loss is substantial, the CCSM2 is a considerable improvement over CSM1. In CSM1, the ocean lost heat during the initialization procedure, and the average ocean temperature was just below  $3^\circ\text{C}$  in

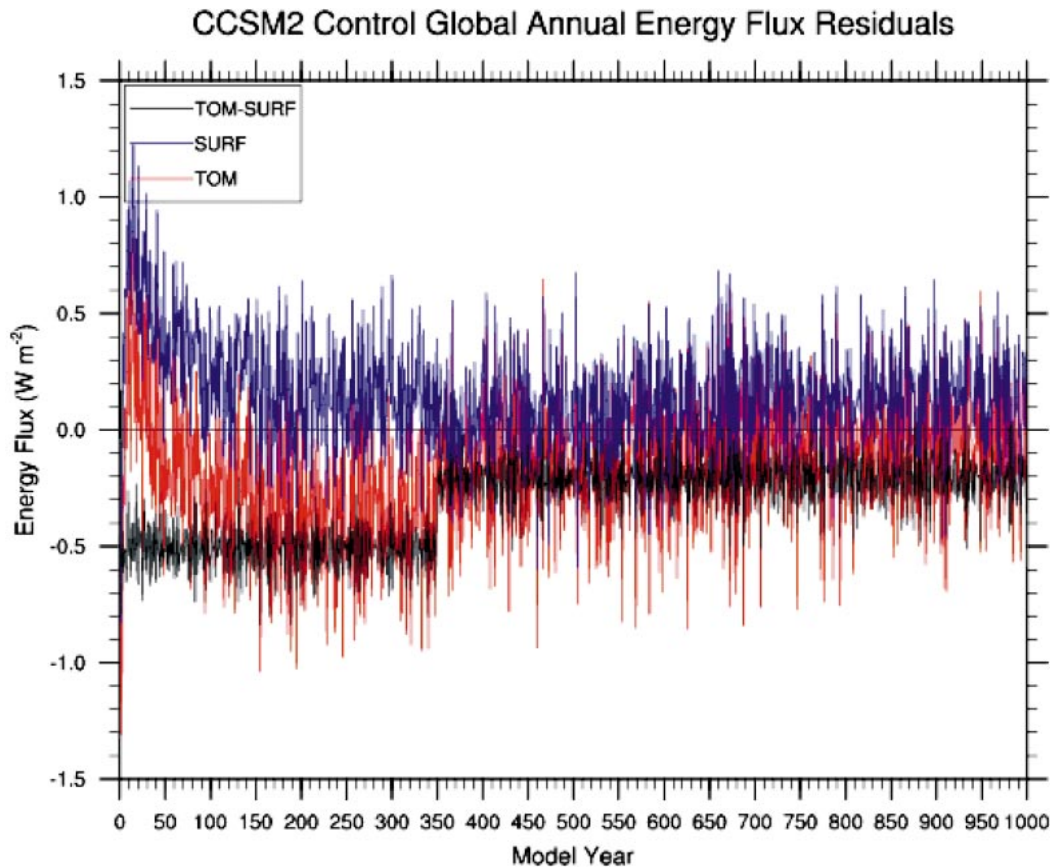


FIG. 2. The net heat balance in  $\text{W m}^{-2}$  at the top of the atmosphere and at the surface, and their difference plotted against time in years. TOM refers to top of model, SURF refers to surface, and TOM–SURF refers to atmospheric fluxes.

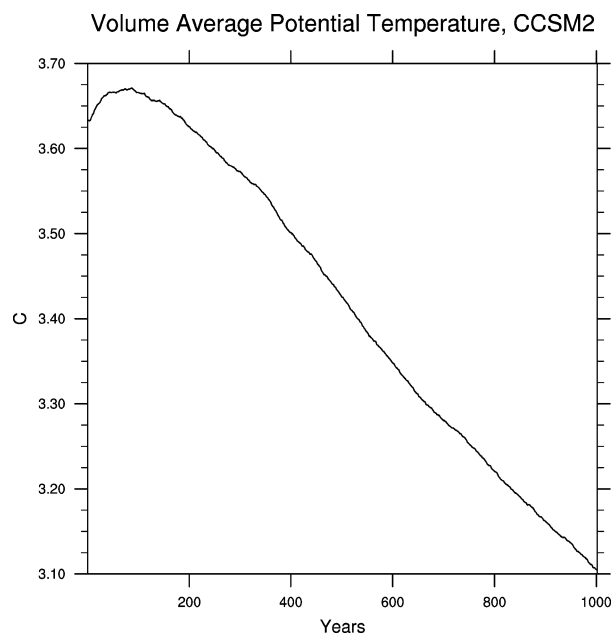


FIG. 3. The volume-averaged potential temperature of the ocean in  $^{\circ}\text{C}$  plotted against time in years.

the initial condition for the coupled simulation. The ocean then lost more heat over the 300-yr coupled run, and the final value was  $2.77^{\circ}\text{C}$  (see Fig. 4 of Bryan 1998).

The second change at year 350 was to correct a bug in the ocean component. The implied salinity change due to frazil ice formation was incorrect because the density of freshwater, not salt water, was being used. This changes the volume-averaged salinity diagnostic from the ocean component, which is shown in Fig. 4. Over the first 350 yr, the ocean salinity reduces partly because of this bug but also because the water content of the deepest soil layer of the land model was reducing. The time scale for the water content of the deepest soil level to reach equilibrium is about 300 yr. The ocean salinity trend was reversed after the bug was corrected. Note the very small-scale range in Fig. 4, with changes in the ocean salinity being on the order of  $10^{-3}$  practical salinity units. This means that freshwater is conserved to a good level of accuracy in CCSM2, although it is not conserved to machine accuracy. The average ocean salinity in CSM1 was absolutely constant because there was no river runoff scheme. Instead, the precipitation over the ocean was multiplied by a factor that ensured that averaged precipitation and evaporation balanced over the global ocean. The third change at year 350 was a very small change in the equation of state used in the ocean component to conform to the final version of McDougall et al. (2003). This resulted in extremely small changes to ocean-alone solutions with and without this change.

The mean SST field from years 961 to 980 is shown in Fig. 5a, and the difference between it and the Levitus/

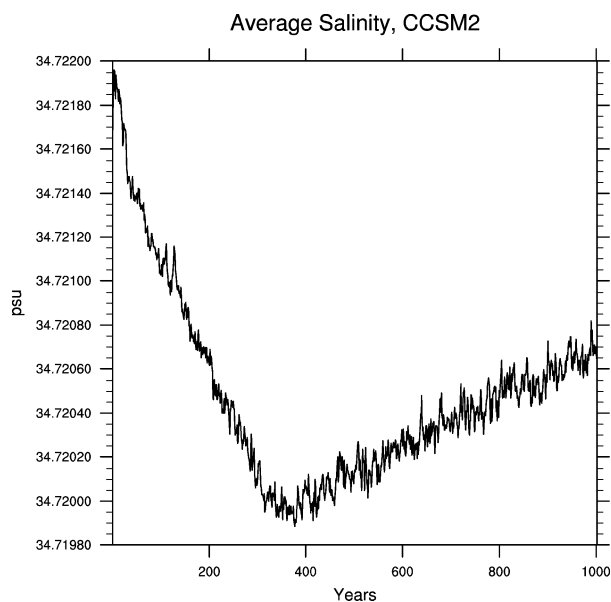


FIG. 4. The volume-averaged salinity of the ocean in practical salinity units (psu) plotted against time in years.

Poles observations is shown in Fig. 5b. The equivalent plot from CSM1 is shown in Fig. 9 of Boville and Gent (1998). Some of the largest SST errors from CSM1 remain in CCSM2. In particular, the equatorial Pacific Ocean has a cold error of more than  $2^{\circ}\text{C}$ , and the warm pool in the west is split by colder SSTs on the equator. The atmospheric precipitation shown in Fig. 6 illustrates the familiar “double ITCZ” problem, where the Southern Hemisphere ITCZ is too strong and extends too far zonally across the Pacific Ocean.

The simulated SST is considerably too warm in the stratus cloud regions off the western coasts of North and South America and Africa. These errors are more than  $5^{\circ}\text{C}$  in small regions right along the coasts and are larger than in CSM1. The cause of this is the increased resolution in the ocean component, since the same resolution exists in the atmosphere component of CCSM2. Straightforward interpolation of the surface wind for the ocean grid box right next to the coast is then more weighted by the wind over land, which is weaker because of the higher drag coefficient over land than over the ocean. Thus, the surface wind stress near the coast is weaker in CCSM2 and is often not directed parallel to the coast. This stress fails to produce coastal upwelling in the ocean component and results in the warm SST errors. Deficiencies in the simulated coastal stratus clouds also contribute to the biases in these regions. The amount of coastal stratus simulated in CCSM2 is between 10% and 20% higher than in CSM1. Despite this improvement in low cloud fraction, CCSM2 still underestimates stratus cloud amount compared to observations.

Another glaring error in the SST field is the greater than  $5^{\circ}\text{C}$  cold error in the central North Atlantic Ocean.

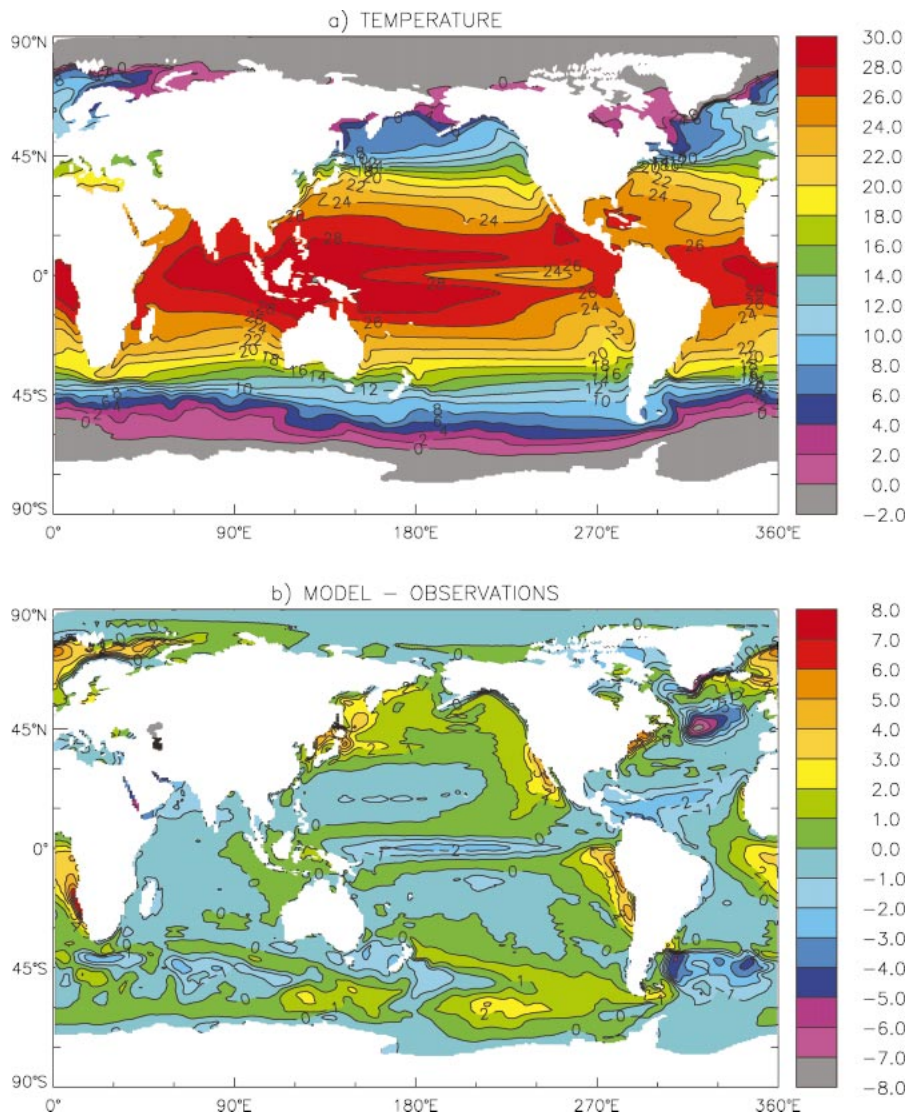


FIG. 5. (a) The mean SST in  $^{\circ}\text{C}$  from years 961 to 980 and (b) the difference in  $^{\circ}\text{C}$  from observations.

The reason is that the simulated Gulf Stream path is too zonal in this region and does not turn northward around the Grand Banks. This is a well-known problem with ocean simulations using an eddy-permitting resolution. So far, this problem has only been solved in regional North Atlantic models using eddy-resolving resolution of  $0.1^{\circ}$  (see Smith et al. 2000). The same happened in the CSM1 simulation, but because of the coarser ocean resolution, the temperature gradient across the Gulf Stream is weaker. This results in a smaller SST error in CSM1. However, the higher-resolution ocean component in CCSM2 does result in thinner and faster western boundary currents. For example, the transport through the Florida Straits in CCSM2 is  $28.5 \text{ Sv}$  ( $1 \text{ Sv} \equiv 10^6 \text{ m}^3 \text{ s}^{-1}$ ), which is much larger than in CSM1 and is within 10% of the observed transport. The average

transport of the Indonesian Throughflow is  $16.8 \text{ Sv}$ , which is a little higher than the average of many disparate observational estimates. However, the transport through two narrow straits in CCSM2 agrees very well with observations. The average outflow through the Strait of Gibraltar is  $0.62 \text{ Sv}$ ; the most recent observational estimate is  $0.67 \pm 0.1 \text{ Sv}$  from Tsimplis and Bryden (2000). The average transport through the Bering Strait is  $0.8 \text{ Sv}$ , which is the same as the estimate of Coachman and Aagaard (1988).

Elsewhere, the SST error is generally less than  $2^{\circ}\text{C}$  and is an improvement over CSM1. In particular, the large cold errors over most of the North Pacific and in the Norwegian Sea have been eliminated. In the Southern Hemisphere, the largest errors occur as a result of displacements in the path of the Antarctic Circumpolar

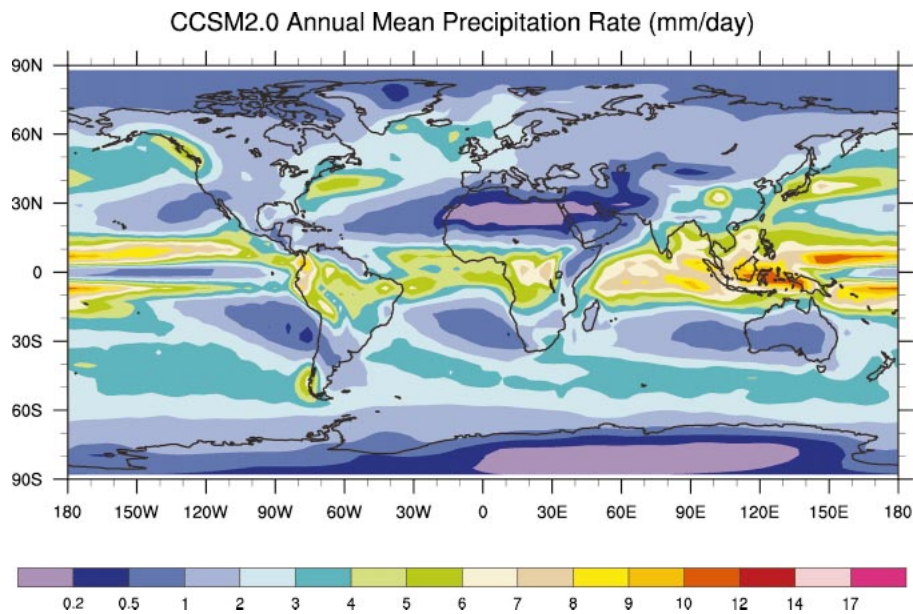


FIG. 6. The annual mean global precipitation rate ( $\text{mm day}^{-1}$ ) averaged from years 961 to 980 of the control simulation.

Current (ACC). The warm error in the Pacific sector of the Southern Ocean has been slowly reducing over the course of the integration. The SST error in this region is  $4^{\circ}\text{C}$  at year 350, but is only  $2^{\circ}\text{C}$  after 1000 yr. This is the only region where there is any significant trend in the SST field over the last 800 yr of the simulation. The reason for this is the very long time scale for the ACC to adjust, because it has significant transport down to 1.5 km. The transport through Drake Passage during

the 1000-yr run is shown in Fig. 7. The transport reduces from 170 Sv at the start to a minimum value of 110 Sv and is slowly increasing at the end of the simulation. The final value of almost 120 Sv is consistent with the best observational estimate of  $130 \pm 13$  Sv (see Whitworth et al. 1982). This is a huge improvement over CSM1, in which the much-too-large drag coefficient between the atmosphere and sea ice caused a too-strong southern thermohaline circulation and a Drake Passage transport of 240 Sv. The drag coefficient was corrected in CSM 1.3 (see Boville et al. 2001), but the Drake Passage transport remained considerably higher than the best observational estimate at 160 Sv.

Figure 8 shows the average sea ice concentration in both hemispheres from the last 10 yr of the control simulation, and the thick solid line is the 10% concentration limit taken from recent observations. The average concentration and aerial coverage in the Northern Hemisphere is quite good, with the sea ice being too extensive only in the Labrador Sea. This is a large improvement over CSM1, in which the sea ice coverage was much too extensive in both the North Pacific and North Atlantic Oceans (see Fig. 6 of Weatherly et al. 1998). However, the annual cycle of concentration in the Arctic is larger than shown in observations, as it was in CSM1 (see Fig. 4 of Weatherly et al. 1998). The average sea ice thickness in the central Arctic in CCSM2 is about 1.5 m, which is too thin compared to the observed value of 2–3 m. However, it is an improvement over CSM1, in which sea ice was between 3 and 6 m in the central Arctic (see Fig. 7 of Weatherly et al. 1998). The Arctic sea ice was also much too thick in CSM 1.3 (see Fig. 16 of Boville et al. 2001).

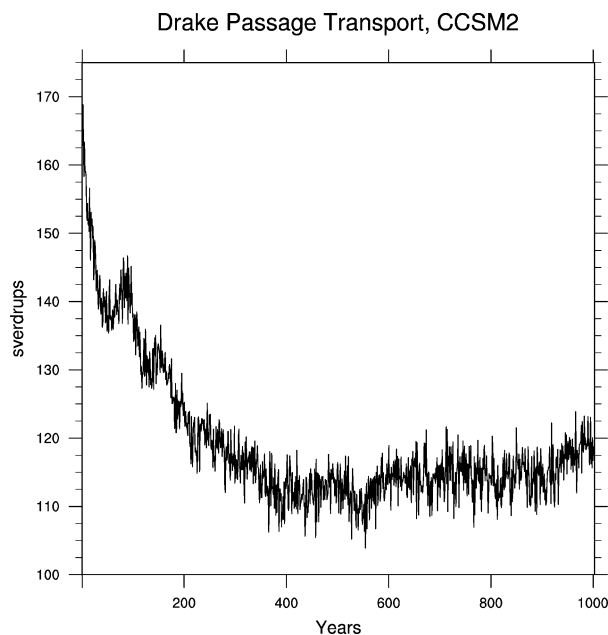


FIG. 7. The transport through Drake Passage in Sv plotted against time in years.

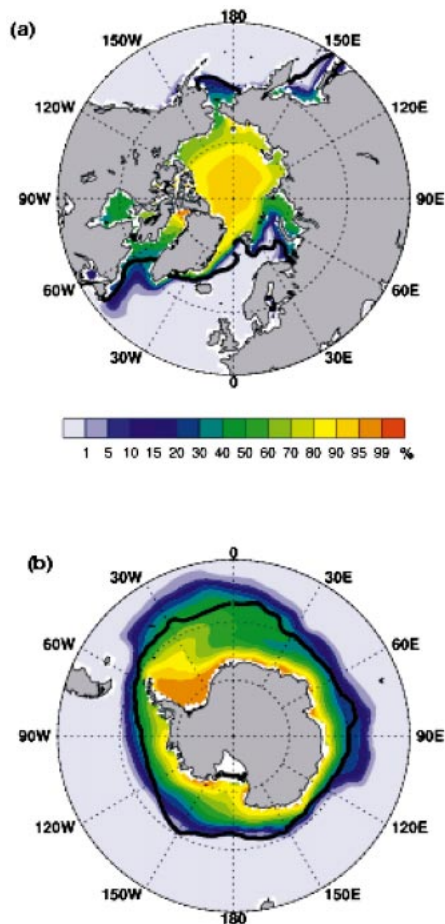


FIG. 8. Average sea ice concentration from years 991 to 1000 for (a) the Arctic and (b) Antarctica. The thick solid lines show the 10% concentration values from observations.

In the Southern Hemisphere, the CCSM2 annual cycle in sea ice concentration is quite realistic, but Fig. 8 shows that the average area is too large. Most of this error occurs in the Atlantic sector of the Southern Ocean. Figure 5 shows that the SSTs are a little cold in this sector, which allows thin ice to grow in the winter. The sea ice thickness distribution around Antarctica is realistic, although the thickest ice on the eastern side of the Antarctic Peninsula is too thick in the simulation. There is a slow but sure increasing trend in the average sea ice area in the Pacific sector of the Southern Ocean over years 350–1000 of the simulation. This corresponds with the very slow cooling trend in the SST in this sector described above. As the SSTs have become more realistic in this sector between the date line and 120°W, so has the sea ice aerial coverage compared to present-day observations. In CSM1, both the average area and annual cycle in area were in good agreement with observations (see Fig. 4 of Weatherly et al. 1998). Thus, the extent of Antarctic sea ice is worse in CCSM2, despite the sea ice component of CCSM2 being much more physically realistic.

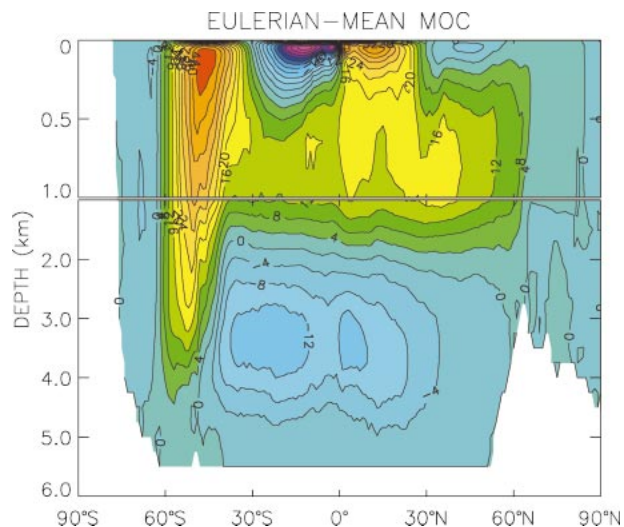


FIG. 9. The mean meridional overturning streamfunction ( $S_v$ ) due to the mean flow averaged over years 961 to 980.

It is well known that the runoff from the Russian rivers flowing north is very important in the freshwater balance of the Arctic Ocean. These runoff flows are realistic, but may be a little high, in the CCSM2 control run. They result in a sea surface salinity field that is quite realistic in the central Arctic but fresh near the Russian coast. The realistic surface salinity, plus much saltier water below 200 m, means that there is a strong halocline in the Arctic Ocean in the simulation. This is a significant improvement over CSM1, in which there was no river runoff and no halocline at all in the Arctic Ocean. A full discussion of the sea ice in CCSM2 can be found in Briegleb et al. (2004).

The total river runoff into the ocean in the control simulation averages to 1.4 Sv. This is about 5% higher than the estimate from observations given in Perry et al. (1996). River runoff is not nearly such a large component to the freshwater budget of other ocean basins, so that incorrect river flows only have a local effect on the sea surface salinity field. For example, the flows in the Amazon and Congo Rivers are considerably too low and high, respectively, in the CCSM2 control run. Thus, the local sea surface salinity is too saline off northeast South America and too fresh off western central Africa. However, overall the sea surface salinity in CCSM2 is considerably improved over that in CSM1, which was much too fresh at the surface (see Fig. 16 of Boville and Gent 1998).

Figure 9 shows the meridional overturning streamfunction from the mean flow averaged over years 961–980. Unfortunately, the streamfunction due to the eddies is not available. However, it is very small, except in the region of 40°–60°S, where it acts to counter the large Deacon cell in the mean flow. The maximum overturning in the Northern Hemisphere is 19.2 Sv, most of which occurs in the North Atlantic. This maximum is

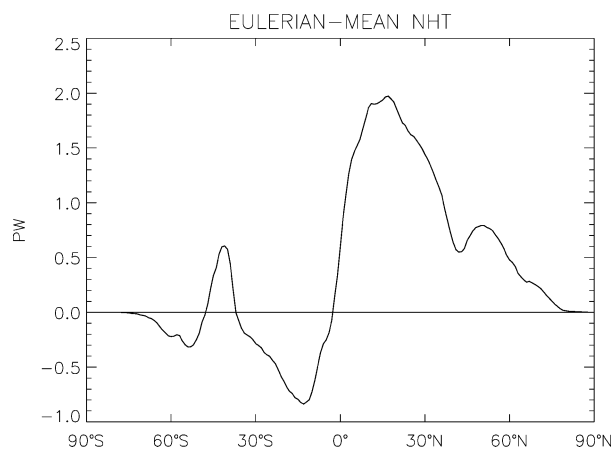


FIG. 10. The mean northward ocean heat transport (PW) due to mean flow averaged over years 961 to 980.

considerably reduced compared to CSM1, where it is 29.2 Sv (see Fig. 8 of Bryan 1998). The CCSM2 value is much more realistic, as the best estimate of the maximum North Atlantic overturning is 17–18 Sv (see, e.g., Fig. 2 of Talley et al. 2003). The deep cell in the Southern Hemisphere is also weaker than in CSM1, but it is probably still too strong. In both CCSM versions, the depth of the zero contour in the Northern Hemisphere is 2.0–2.5 km, which is considerably too shallow compared to observations. This is a common error in  $z$  coordinate ocean climate models. It is caused by the poor representation of overflow currents flowing down the topography and by the overflow into the North Atlantic being less dense than in reality.

The northward heat flux due to the mean ocean circulation is shown in Fig. 10. The maximum poleward heat transports are 2.0 PW in the north and 0.85 PW in the south. These are very realistic compared to the most recent estimates using observations (see, e.g., Fig. 6 of Trenberth and Caron 2001). The eddy heat transport is largest around 40°S and is poleward, so that the total heat transport is probably poleward throughout the Southern Hemisphere. The ocean heat transport in CCSM2 is very similar to that in CSM1, which is shown in Fig. 9 of Bryan (1998).

The zonally averaged temperature and salinity differences from the observations used as initial conditions at the end of the control run are shown in Fig. 11. Much of the deep ocean is just over 1°C cold, but the deep salinity is within 0.2 psu of observations. Both drifts are considerably smaller than at the end of the 300-yr CSM1 control integration (see Fig. 7 of Bryan 1998). The largest temperature error is 3°–4°C at 65°–75°N between 200-m and 1-km depths. This error is significant but is again smaller than in CSM1. The largest salinity errors are near the surface in the Northern Hemisphere. The large temperature error near 10°S at 100-m depth is due to a vertical displacement of the thermocline caused by the erroneous winds associated with

the Southern Hemisphere component of the double ITCZ.

There have been a number of improvements in the atmospheric simulation of CCSM2 compared to that of CSM1. The improvement in zonal mean annual mean thermal structure is shown in Fig. 12. The bias in the CSM1 zonal mean temperature relative to the National Centers for Environmental Prediction (NCEP)–NCAR reanalysis is shown in Fig. 12b. Near the surface, the Northern Hemisphere polar region is colder by up to 8 K compared to the analyses, and the model is also cold over Antarctica. In the tropical region, the lower to middle stratosphere is too warm by up to 6 K compared to the reanalysis. The difference between the CCSM2 simulation and the reanalysis is shown in Fig. 12a. The new version of the coupled model is warmer than the reanalysis in the Northern Hemisphere polar region. Thus, the new version of the model has addressed the cold bias at high latitudes near the surface and has even overcompensated for the bias. In the tropical region, the new model is colder than CSM1 near 70 hPa. At the tropical tropopause the new model is now too cold compared to the reanalysis and to radiosonde data in the Tropics. The tropical tropopause cold bias is as large as 6 K. This is a significant bias in applying the model to middle-atmosphere research, since this has serious implications for lower-stratospheric water vapor mixing ratios.

As noted above, a significant change in the CCSM2 atmospheric component is in the treatment of longwave water vapor continuum. The clear-sky outgoing longwave radiation to space is shown in Fig. 13. In the Tropics, the CCSM2 clear-sky flux is much closer to the Earth Radiation Budget Experiment (ERBE) observations. At high latitudes, the CCSM2 flux is too large compared to ERBE and CSM1.3. This bias, however, is due to the warm bias at high latitudes. The zonal annual mean surface air temperature over land is shown in Fig. 14. In terms of the zonal mean, CSM1 was much closer to the observational data, while CCSM2 is too warm by up to 8 K near both poles. These excessive temperatures lead to an excess emission of clear-sky longwave radiation to space.

The geographic distribution of difference in annual surface air temperature over land is shown in Fig. 15. The difference between CSM1 and the observational data is shown in Fig. 15b. In general, the simulated land temperatures are too cold. The United States is cold by up to 6 K in the southwest. In the region of the Sahara, the simulated temperatures are cold by as much as 10 K. The only region that is significantly warmer than the observations is located in northern Greenland and Canada. The comparison of CCSM2 against observations in Fig. 15a indicates that the newer model is warmer in virtually every region, with the largest increase in temperature at high latitudes. This increase in temperature is due to changes in cloud properties in the atmospheric component and changes in the land component. Both of these new components predict warmer surface air tem-

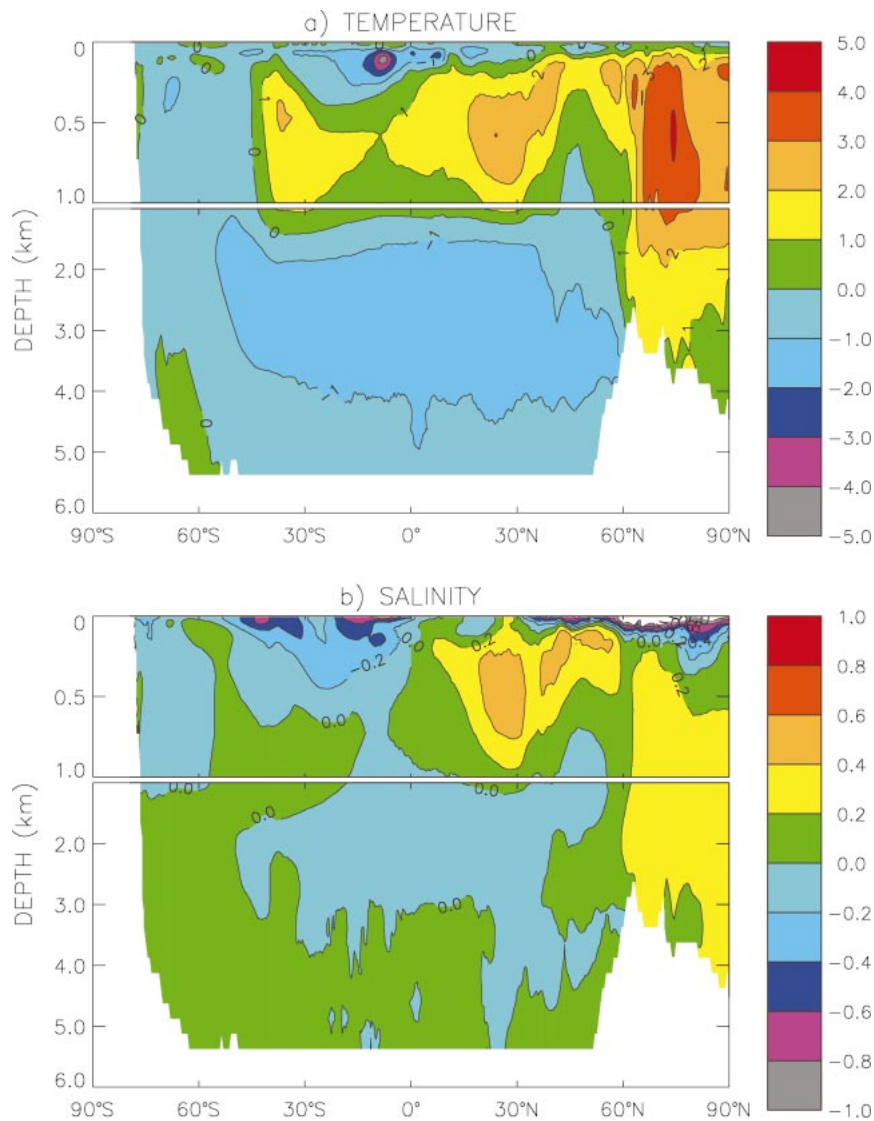


FIG. 11. (a) The zonally averaged mean potential temperature ( $^{\circ}\text{C}$ ) from years 961 to 980 minus observations; (b) the zonally averaged salinity (psu) from years 961 to 980 minus observations.

peratures when run in the uncoupled mode. Coupling the components leads to even warmer temperatures. In most regions, excluding the high latitudes, the increase in surface air temperature in CCSM2 has removed much of the initial temperature bias. However, at high latitudes, CCSM2 is now significantly warmer (locally by up to 12 K) than the observations. Thus the new model has overcompensated for the surface air temperature bias in CSM1.

Aspects of the hydrologic cycle have also changed from CSM1 to CCSM2. The change in geographic distribution of precipitable water is shown in Fig. 16. The original bias in precipitable water in CSM1 compared to the National Aeronautics and Space Administration (NASA) Water Vapor Project (NVAP; Randel et al. 1996) observations (Fig. 16b) indicates a significant dry

bias in the Tropics, with biases as large as 15 mm in column water vapor. The difference between CCSM2 and the NVAP data (Fig. 16a) indicates that some of the tropical dry bias has been addressed in CCSM2. Note that the excessive moisture in the Pacific subsidence region off of South America has also been reduced in the new version of the coupled model. Given that water vapor is the most important greenhouse gas in the earth's atmosphere, it is encouraging to see that the simulation of this constituent has improved in CCSM2.

Perhaps the most important aspect of the hydrologic cycle is the rate of precipitation. The geographic distribution in differences of precipitation rate is shown in Fig. 17. The bias in CSM1 compared to the Global Precipitation Climatology Project (GPCP; Adler et al.

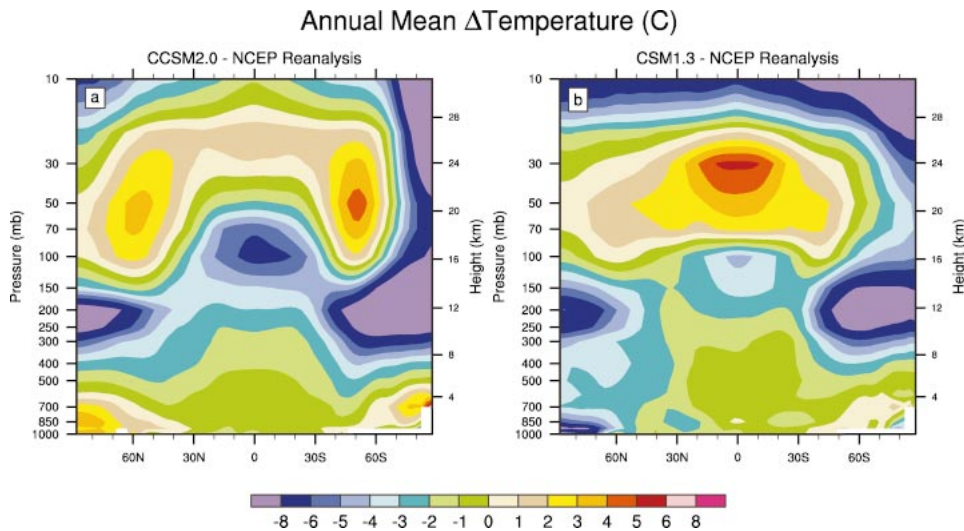


FIG. 12. Difference in zonal mean annual mean temperature (K) between (a) CCSM2 minus NCEP–NCAR reanalysis and (b) CSM1 minus NCEP–NCAR reanalysis.

2003) observations (Fig. 17b) shows, in general, an overprediction of rainfall in the Tropics. This model, as in many coupled models, simulates a double ITCZ structure. In the western tropical Pacific, CSM1 predicts too much rainfall north of the equator and too little rainfall south of the equator, indicating a northward shift in rainfall compared to the observations. In the eastern equatorial Pacific, there is excessive rainfall at 15°S, which is a manifestation of the double ITCZ structure. There is excessive rainfall in the western Indian Ocean and a southward shift in the ITCZ in the tropical At-

lantic. Over land regions, there is excessive rainfall in central Africa and too little precipitation in Brazil. These biases in precipitation rate manifest in the predicted river runoff and hence affect surface salinity in the oceans.

CCSM2 suffers from many of the biases existing in CSM1 in terms of precipitation rate. There are two regions over the ocean where the precipitation distribution has improved in CCSM2 compared to CSM1. Over Indonesia and the Pacific warm pool region, the CCSM2 simulated rainfall is lower by up to 4–5 mm day<sup>-1</sup> compared to CSM1.3 (Fig. 17a), and in the eastern Pacific,

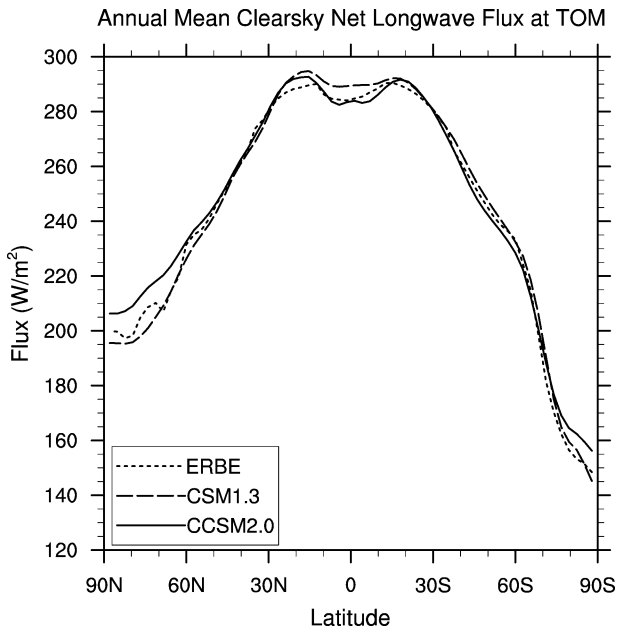


FIG. 13. Zonal mean annual clear-sky outgoing longwave flux ( $W m^{-2}$ ) for ERBE observations (dotted), CSM1 (dashed), and CCSM2 (solid).

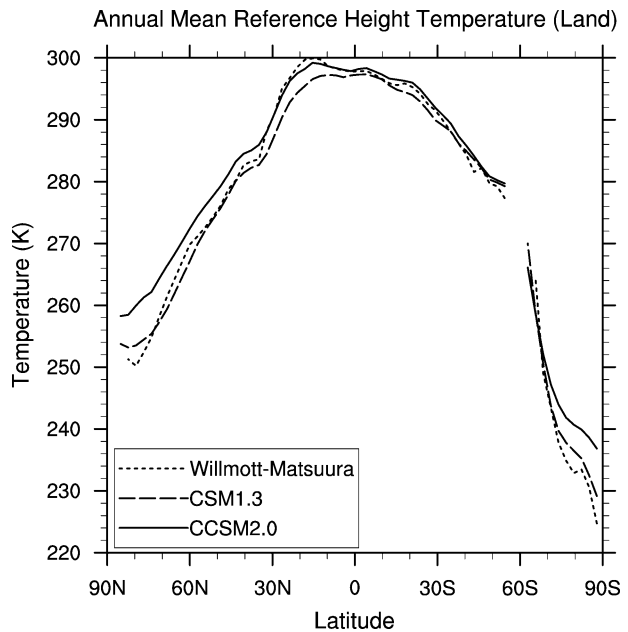


FIG. 14. Zonal mean annual land surface air temperature (K) for observations (dotted), CSM1 (dashed), and CCSM2 (solid).

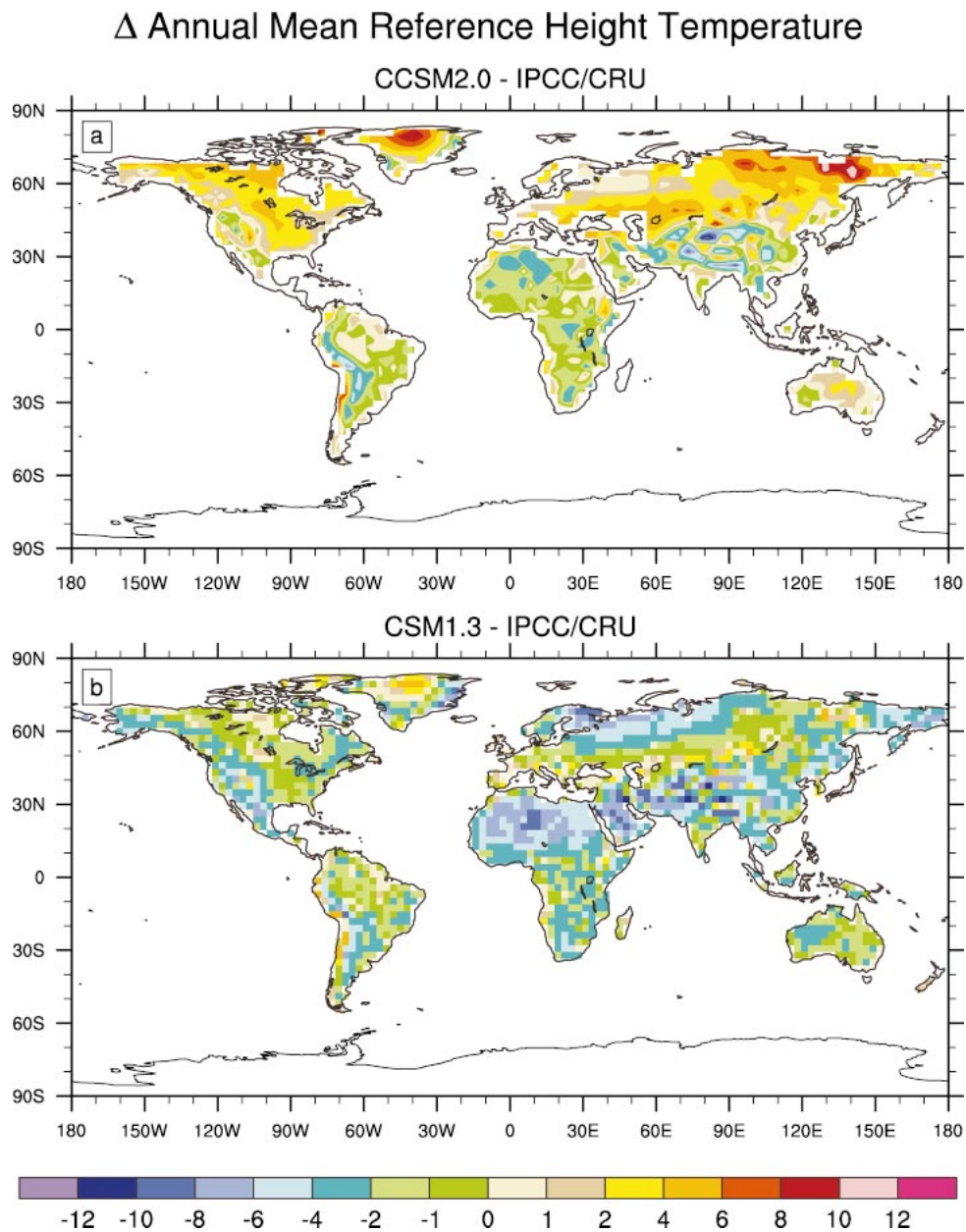


FIG. 15. Geographic distribution of difference in annual mean surface air temperature (K) between (a) CCSM2 and observations, and (b) CSM1 and observations.

the excessive rainfall at  $15^{\circ}\text{S}$  has decreased by more than  $6 \text{ mm day}^{-1}$ , leading to a less severe double ITCZ structure. The underestimate of precipitation at  $5^{\circ}\text{N}$  in this region, shown in Fig. 17b, for CSM1 is also alleviated in CCSM2 (see Fig. 17a). Over land, the rainfall in central Africa is now much reduced and closer to the observations, and there has been an increase in rainfall in eastern Brazil, again reducing the bias that exists in CSM1 in this region. Thus, overall the precipitation rate in CCSM2 is superior to that simulated by CSM1.

An important measure of climate change is a model's sensitivity to increased atmospheric carbon dioxide. One

measure of climate sensitivity is the equilibrium change in global annual mean surface temperature due to an instantaneous doubling of  $\text{CO}_2$ . The atmospheric, land, and thermodynamic sea ice components of CCSM2 have been coupled to a slab ocean model to perform these equilibrium simulations. The slab ocean component is described in Kiehl et al. (1996). Briefly the model employs an annual mean, spatially varying prescribed mixed layer depth and monthly mean, spatially varying specified ocean heat fluxes, such that the control simulation represents a realistic distribution of surface temperature. This version of CCSM2 has been integrated

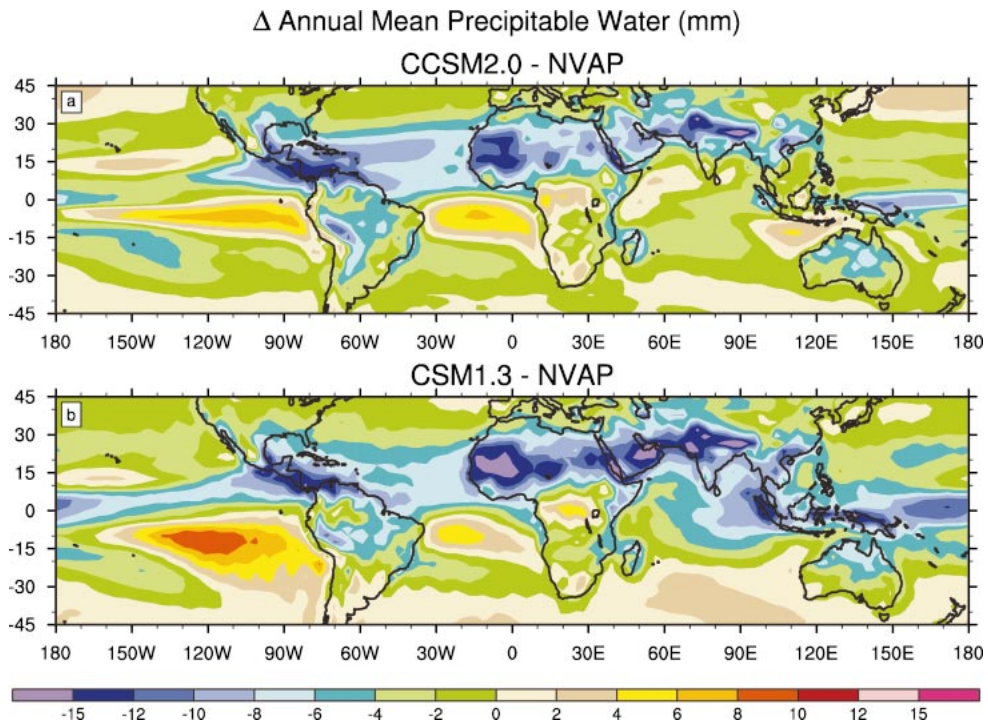


FIG. 16. Geographic distribution of difference in annual mean tropical precipitable water (mm) between (a) CCSM2 and NVAP observations, and (b) CSM1 and NVAP observations.

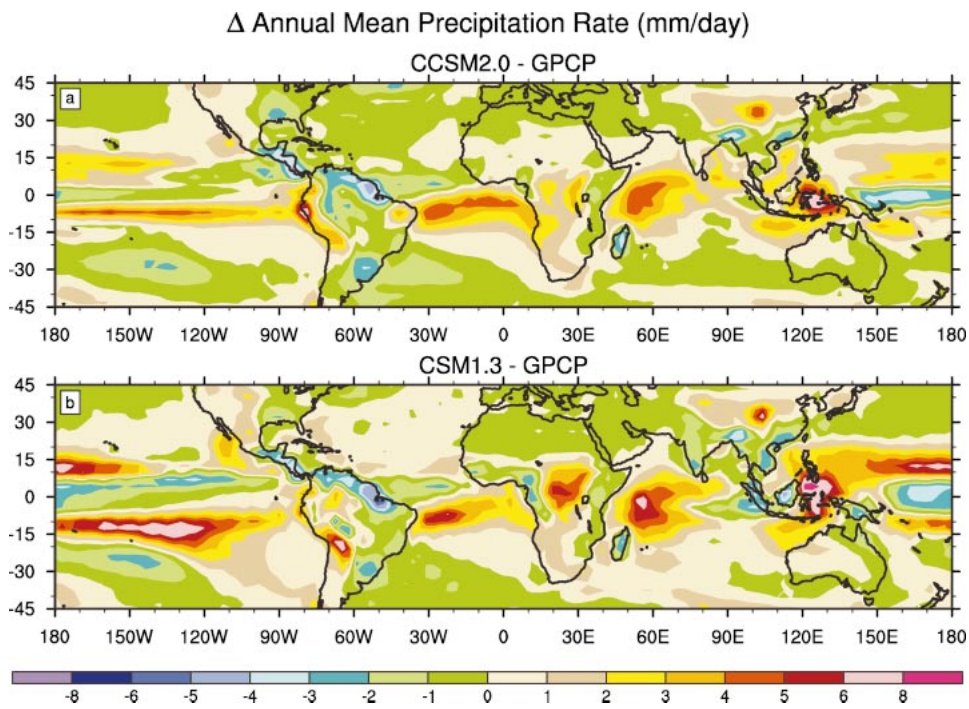


FIG. 17. Geographic distribution of difference in annual mean tropical precipitation rate ( $\text{mm day}^{-1}$ ) between (a) CCSM2 and GPCP observations, and (b) CSM1 and GPCP observations.

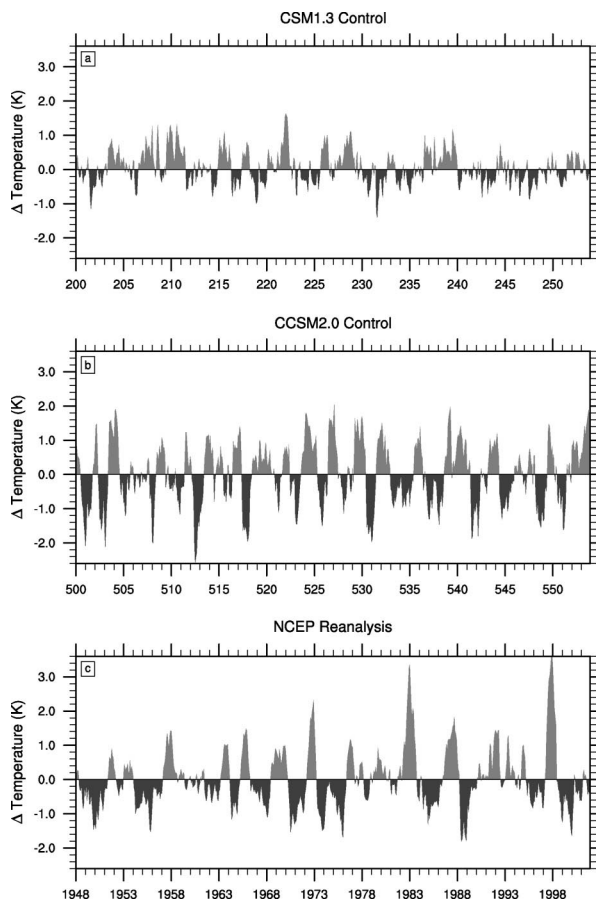


FIG. 18. Niño-3 time series of SST ( $^{\circ}$ C) anomalies for (a) CSM1, (b) CCSM2, and (c) NCEP-NCAR reanalysis.

for both a control level of  $\text{CO}_2$  (355 ppmv) and 2 times this amount, where each simulation is 40 yr in length. The climate sensitivity of CCSM2 from these integrations is 2.2 K, which is slightly larger than the value of 2.0 K obtained for CSM1.

#### 4. Interannual variability

The largest interannual signal in the climate system is the El Niño–Southern Oscillation (ENSO). We have described above the quite large errors in the mean climate of the tropical Pacific in the control simulation. Given these errors, it is not surprising that the ENSO variability also shows considerable differences compared to observed ENSO events. Despite these mean state errors, the coupled model does exhibit tropical variability and amplitude, and the phase of this variability is significantly different between CCSM2 and CSM1.

ENSO variability is most frequently diagnosed by the time series of SST anomalies in the Niño-3 area,  $5^{\circ}\text{S}$ – $5^{\circ}\text{N}$ ,  $90^{\circ}$ – $150^{\circ}\text{W}$ , which is shown in Fig. 18. Shown are the anomaly in SST from 54 yr of reanalysis (1948–2001) and the anomalies from the last 54-yr period of the control simulations of CSM1 and CCSM2. The am-

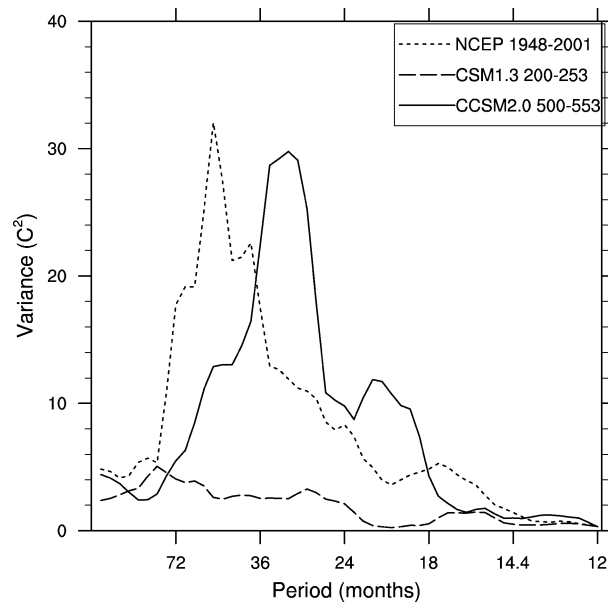


FIG. 19. Power spectrum of monthly mean Niño-3 SST anomalies for CCSM2 (solid), CSM1 (dashed), and NCEP-NCAR reanalysis (dotted).

plitude of the CCSM2 Niño-3 time series (Fig. 18b) is smaller than reality, with the largest events being just over  $\pm 2^{\circ}\text{C}$  and an rms value of just less than  $1^{\circ}\text{C}$ . The amplitude of the CSM1 Niño-3 variability is much weaker than that of CCSM2 (by more than a factor of 2). Figure 19 shows the power spectra of these ENSO time series. The peak of the frequency spectrum of the CCSM2 Niño-3 index is between 2 and 3 yr, rather than the observed broad peak of between 3 and 7 yr. While the peak in power in CSM1 is closer to the observed value, it is barely significant at the 95% confidence level.

In terms of the geographic pattern (not shown) both models' ENSO variability is much too strong farther to the west along the Pacific equator, where the amplitude is comparable to that in the Niño-3 area. This is a direct consequence of the cold tongue being too strong and extending too far west (see Fig. 5), generating too much SST variability when equatorial ocean upwelling switches on and off. Figure 5 also shows that the mean SST along the equator in the far eastern Pacific is too warm. Just as in CSM1, the annual cycle of SST in this area shows a dominant semiannual signal, whereas observations show a dominant annual signal.

However, an interesting aspect of the Niño-3 time series is that it shows variability on the 50–100-yr time scale. The 2–3-yr time scale shows up clearly in most of the 1000-yr run. However, the Niño-3 time series between years 530 and 570 shows longer time-scale variability and is much more in line with observations over the last 50 yr. It would be instructive to analyze why ENSOs were different during this relatively brief period, but that is beyond the scope of the present paper.

In contrast, the CCSM2 has a realistic North Atlantic

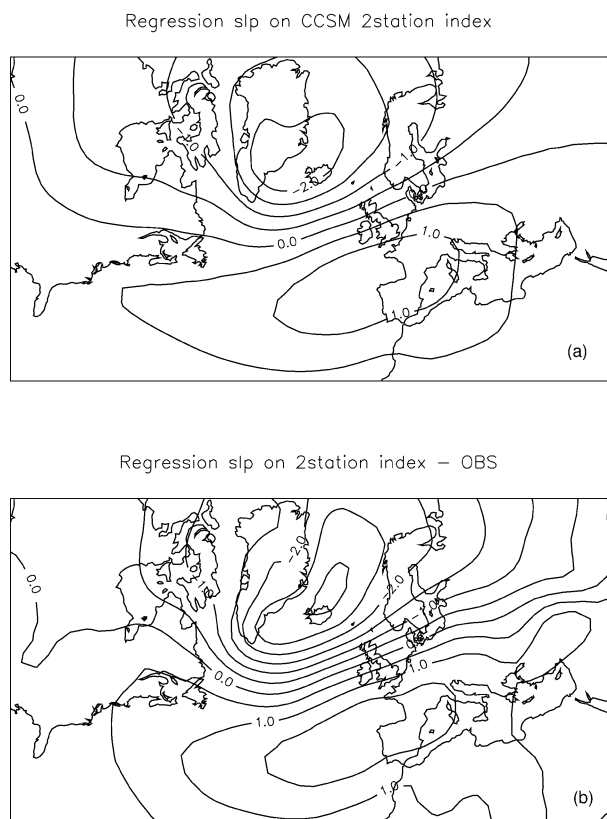


FIG. 20. The regression of sea level pressure on the two-station index of the NAO. (a) The control simulation between years 351 and 900, and (b) NCEP–NCAR reanalysis data for 1950–98.

Oscillation (NAO). The NAO index is usually defined as the difference in surface atmospheric pressure between Portugal and Iceland. Figure 20 shows the regression of sea level pressure on this two-station index from both the control run between the years 351 and 900 and the NCEP–NCAR reanalysis between 1950 and 1998. The figure shows that CCSM2 realistically captures the spatial pattern of the NAO, with the opposite centers of action occurring near Iceland and the Iberian Peninsula. Additional analysis shows that the amplitude is a little weak compared to observations. However, the amplitude discrepancy could be because the comparison is between a control run with fixed external forcings, such as the solar constant and the  $\text{CO}_2$  concentration, and reality, where the climate forcings are changing.

In addition, Holland (2003) documents that the variability in the Arctic sea ice and the surrounding ocean forced by wind changes associated with the NAO are also realistic in the control simulation. A high NAO index has stronger westerlies across the North Atlantic, forcing stronger transport of warm Atlantic water into the Greenland–Iceland–Norwegian and Barents Seas. This, in turn, reduces the sea ice cover in these seas, but there is more extensive sea ice cover in the Labrador Sea. This can change the location of the deep-water formation that drives the thermohaline circulation in the

North Atlantic. More details of the NAO and the changes to the sea ice and ocean in the CCSM2 control run can be found in Holland (2003).

## 5. Discussion and conclusions

CCSM2 has many improvements over CSM1. They include

- a completely new, state-of-the-art sea ice component with a much-improved ice rheology, ice thickness distribution, and thermodynamics;
- a completely new land component with new formulations of ground and vegetation fluxes, biogeophysical processes, and snowpack;
- a realistic, high-resolution river runoff scheme;
- a displaced Northern Hemisphere pole into Greenland for the much finer ocean and sea ice grids, which means that no Fourier filtering is required in the Arctic Ocean and that the Bering Strait is open;
- a new prognostic cloud water, a new cloud overlap parameterization, and an updated water vapor emissivity/absorptivity scheme included in the new atmosphere component (CAM2.0).

These changes have led to a much-improved simulation of the Arctic in CCSM2. The mean sea ice distribution is very realistic; there is a realistic halocline in the Arctic Ocean and flow through the Bering Strait compared to CSM1. This has led to realistic interannual variability in the Arctic sea ice and ocean (see Holland 2003).

In terms of the atmospheric simulation, there is an improvement in the simulated tropical precipitable water magnitude and spatial distribution. The zonal mean atmospheric thermal structure is much improved in CCSM2 over CSM1 in that CCSM2 no longer has a severe cold bias near the polar surface. There is also a significant improvement in the downward longwave clear-sky radiation due to the incorporation of a new continuum formulation. The equilibrium climate sensitivity of CCSM2 is 2.2 K, which is slightly larger than that of CSM1.

The higher ocean horizontal resolution gives faster and narrower western boundary currents and equatorial currents compared to CSM1. The transport through Drake Passage is much better than in CSM1. This results from a correct air–sea ice drag coefficient and improved implementation of ocean parameterizations. The strength of the thermocline circulation in the North Atlantic is considerably reduced compared to CSM1 and is much closer to observations. The ocean poleward heat transport also compares well to observed estimates. The deep ocean temperature and salinity errors are significant after 1000 yr in the CCSM2 but are much smaller than in the CSM1.

The ocean, sea ice, and land components were specifically designed for massively parallel computers. The CCSM2 runs quite efficiently on these machines but still

needs work to enable it to run efficiently on more than the order of 150 processors.

There are also a number of aspects where CCSM2 has not improved over CSM1. They include the following:

- The mean climate of the tropical Pacific. There is a double ITCZ, the cold tongue reaches too far west into the western Pacific Ocean, and the SSTs are much too warm in the stratus regions off South America. Consequently, the model ENSOs have too much variability in the west, and the peak of the spectrum is too high at 2–3 yr.
- The Gulf Stream does not go north around the Grand Banks; instead it heads northeast across the Atlantic toward Europe. This leads to large errors in SST and sea surface salinity in the central North Atlantic. The higher ocean resolution has not helped the Gulf Stream path, but it does allow sharper gradients across the Gulf Stream. This leads to larger local errors than in the lower resolution CSM1.
- The sea ice in the Arctic is too thin compared to observations, and the thickest ice is on the Russian side, rather than the Canadian side. This was also true in CSM1 and is probably caused by incorrect surface winds. The sea ice distribution off Antarctica is a little worse than in CSM1 because there is too much very-thin ice too far north in the Atlantic sector of the Southern Ocean. However, the amplitude of the annual cycle in Antarctic sea ice is realistic in CCSM2.
- The tropical tropopause is too cold by as much as 6 K, which is a degradation over what was simulated in CSM1. The cause of this degradation is a result of changes in a number of the physical parameterizations.
- The land surface has a significant warm bias at high latitudes. Changes in both the atmosphere and land components from CSM1 to CCSM2 have compounded this effect.

The preceding paragraphs list several deficiencies in the control simulation of CCSM2. Therefore, these are the aspects of the coupled model that need to be worked on in the future. The high-latitude warm bias in surface temperatures limits the applicability of the model to future climate change, since polar amplification due to increased greenhouse gases is a generic feature in coupled models. Thus it is important to address the deficiencies in this aspect of CCSM2 in future model development. In the Tropics, the model continues to have excessively warm temperatures in eastern boundary regions of coastal upwelling. This has been identified as a contributing element to the double ITCZ problem in the deep Tropics. Improved simulation of marine stratocumulus and the atmospheric circulation along coastal regions should help to alleviate this bias.

In terms of variability, the highest priority must be to improve the simulation in the tropical Pacific and the ENSO interannual variability. The poor simulation of ENSO means that the present model is easily criticized

when used to simulate future scenarios of the earth's climate. In our view, many of the present deficiencies require improved component parameterizations and will not be overcome just by additional resolution. Higher resolution will be used in the future as computers continue to get more powerful, but parameterization improvements are also needed. This requires input from a wide variety of disciplines and scientists. The CCSM project welcomes and encourages participation through the mechanism of its nine working groups.

*Acknowledgments.* The control simulation was carried out at NERSC, which is funded by the Department of Energy. This project would not have been completed without the unwavering support of the program managers, Jay Fein of NSF and Dave Bader of DOE. We also thank Mark Stevens and Christine Shields for generating many of the figures and Lawrence Buja for verifying model configuration details. The DOE Atmospheric Radiation Measurements (ARM) program supported J.T.K. for this research.

#### REFERENCES

- Adler, R. F., and Coauthors, 2003: The version-2 Global Precipitation Climatology Project (GPCP) monthly precipitation analysis (1979–present). *J. Hydrometeor.*, **4**, 1147–1167.
- Bitz, C. M., and W. H. Lipscomb, 1999: An energy-conserving thermodynamic model of sea ice. *J. Geophys. Res.*, **104**, 15 669–15 677.
- , M. M. Holland, M. Eby, and A. J. Weaver, 2001: Simulating the ice-thickness distribution in a coupled climate model. *J. Geophys. Res.*, **106**, 2441–2463.
- Bonan, G. B., 1998: The land surface climatology of the NCAR Land Surface Model coupled to the NCAR Community Climate Model. *J. Climate*, **11**, 1307–1326.
- , K. W. Oleson, M. Vertenstein, and S. Levis, 2002: The land surface climatology of the Community Land Model coupled to the NCAR Community Climate Model. *J. Climate*, **15**, 3123–3149.
- Boville, B. A., and P. R. Gent, 1998: The NCAR Climate System Model, version one. *J. Climate*, **11**, 1115–1130.
- , J. T. Kiehl, P. J. Rasch, and F. O. Bryan, 2001: Improvements to the NCAR CSM-1 for transient climate simulations. *J. Climate*, **14**, 164–179.
- Branstetter, M. L., and D. J. Erickson III, 2003: Continental runoff dynamics in the Community Climate System Model (CCSM-2) control simulations. *J. Geophys. Res.*, **108**, 4550, doi:10.1029/2002JD003212.
- Briegleb, B. P., E. C. Hunke, C. M. Bitz, W. H. Lipscomb, M. M. Holland, J. L. Schramm, and R. E. Moritz, 2004: The sea ice simulation of the Community Climate System Model, version two. NCAR Tech. Note NCAR/TN-45+STR, 34 pp.
- Bryan, F. O., 1998: Climate drift in a multicentury integration of the NCAR Climate System Model. *J. Climate*, **11**, 1455–1471.
- Clough, S. A., F. X. Kneizys, and R. W. Davies, 1989: Line shape and the water vapor continuum. *Atmos. Res.*, **23**, 229–241.
- Coachman, L. K., and K. Aagaard, 1988: Transports through Bering Strait: Annual and interannual variability. *J. Geophys. Res.*, **93**, 15 535–15 539.
- Collins, W. D., 2001: Parameterization of generalized cloud overlap for radiative calculations in general circulation models. *J. Atmos. Sci.*, **58**, 3224–3242.
- , J. K. Hackney, and D. P. Edwards, 2002: An updated parameterization for infrared emission and absorption by water vapor

- in the National Center for Atmospheric Research Community Atmosphere Model. *J. Geophys. Res.*, **107**, 4664, doi:10.1029/2001JD001365.
- Dickinson, R. E., A. Henderson-Sellers, and P. Kennedy, 1993: Biosphere-atmosphere Transfer Scheme (BATS) version 1e as coupled to the NCAR community climate model. NCAR Tech. Note NCAR/TN-387+STR, Boulder, CO, 72 pp.
- Gent, P. R., and J. C. McWilliams, 1990: Isopycnal mixing in ocean circulation models. *J. Phys. Oceanogr.*, **20**, 150–155.
- Griffies, S. M., 1998: The Gent-McWilliams skew flux. *J. Phys. Oceanogr.*, **28**, 831–841.
- Holland, M. M., 2003: The North Atlantic Oscillation–Arctic Oscillation in the CCSM2 and its influence on Arctic climate variability. *J. Climate*, **16**, 2767–2781.
- Hunke, E. C., and J. K. Dukowicz, 1997: An elastic–viscous–plastic model for sea ice dynamics. *J. Phys. Oceanogr.*, **27**, 1849–1867.
- Kiehl, J. T., J. J. Hack, G. B. Bonan, B. A. Boville, B. P. Briegleb, D. L. Williamson, and P. J. Rasch, 1996: Description of the NCAR Community Climate Model (CCM3). NCAR Tech. Note NCAR/TN-420+STR, Boulder, CO, 152 pp.
- , —, —, —, D. L. Williamson, and P. J. Rasch, 1998: The National Center for Atmospheric Research Community Climate Model: CCM3. *J. Climate*, **11**, 1131–1149.
- , T. L. Schneider, R. W. Portmann, and S. Solomon, 1999: Climate forcing due to tropospheric and stratospheric ozone. *J. Geophys. Res.*, **104**, 31 239–31 254.
- Large, W. G., J. C. McWilliams, and S. C. Doney, 1994: Oceanic vertical mixing: A review and a model with a nonlocal boundary layer parameterization. *Rev. Geophys.*, **32**, 363–403.
- Levitus, S., R. Burgett, and T. P. Boyer, 1994: *Salinity*. Vol. 3, *World Ocean Atlas 1994*, NOAA Atlas NESDIS 3, 99 pp.
- Lipscomb, W. H., 2001: Remapping the thickness distribution in sea ice models. *J. Geophys. Res.*, **106**, 13 989–14 000.
- McDougall, T. J., D. R. Jackett, D. G. Wright, and R. Feistel, 2003: Accurate and computationally efficient algorithms for potential temperature and density of seawater. *J. Atmos. Oceanic Technol.*, **20**, 730–741.
- Perry, G., P. Duffy, and N. Miller, 1996: An extended data set of river discharges for validation of general circulation models. *J. Geophys. Res.*, **101**, 21 339–21 349.
- Randel, D. L., T. H. vonder Haar, M. A. Ringerud, G. L. Stephens, T. J. Greenwald, and C. L. Combs, 1996: A new global water vapor dataset. *Bull. Amer. Meteor. Soc.*, **77**, 1233–1254.
- Rasch, P. J., and J. E. Kristjansson, 1998: A comparison of the CCM3 model climate using diagnosed and predicted condensate parameterizations. *J. Climate*, **11**, 1587–1614.
- Smagorinsky, J., 1963: General circulation experiments with the primitive equations. *Mon. Wea. Rev.*, **91**, 99–164.
- Smith, R. D., and P. R. Gent, Eds., cited 2002: Reference manual for the Parallel Ocean Program (POP); ocean component of the Community Climate System Model (CCSM-2). [Available online at <http://www.cesm.ucar.edu/models/ccsm2.0.1/pop/>.]
- , and J. C. McWilliams, 2003: Anisotropic horizontal viscosity for ocean models. *Ocean Modell.*, **5**, 129–156.
- , J. K. Dukowicz, and R. C. Malone, 1992: Parallel ocean general circulation modeling. *Physica D*, **60**, 38–61.
- , M. E. Meltrud, F. O. Bryan, and M. W. Hecht, 2000: Numerical simulation of the North Atlantic Ocean at  $\frac{1}{10}^\circ$ . *J. Phys. Oceanogr.*, **30**, 1532–1561.
- Steele, M., R. Morley, and W. Ermold, 2001: PHC: A global ocean hydrography with a high-quality Arctic Ocean. *J. Climate*, **14**, 2079–2087.
- Talley, L. D., J. L. Reid, and P. E. Robbins, 2003: Data-based meridional overturning streamfunctions for the global ocean. *J. Climate*, **16**, 3213–3226.
- Trenberth, K. E., and J. M. Caron, 2001: Estimates of meridional atmosphere and ocean heat transports. *J. Climate*, **14**, 3433–3443.
- Tsimplis, M. N., and H. L. Bryden, 2000: Estimation of transports through the Strait of Gibraltar. *Deep-Sea Res.*, **47**, 2219–2242.
- Weatherly, J. W., B. P. Briegleb, W. G. Large, and J. A. Maslanik, 1998: Sea ice and polar climate in the NCAR CCSM. *J. Climate*, **11**, 1472–1486.
- Whitworth, T., W. D. Nowlin, and S. J. Worley, 1982: The net transport of the Antarctic Circumpolar Current through Drake Passage. *J. Phys. Oceanogr.*, **12**, 960–971.
- Zeng, X., 2001: Global vegetation root distribution for land modeling. *J. Hydrometeorol.*, **2**, 525–530.